Electronic Supplementary Material (ESI) for Inorganic Chemistry Frontiers.

High-Efficient Electrochemical Synthesis of low-Nuclearity Copper-clusters-based metal-organic framework for size-selective oxidation of alcohols

Zixuan Huang, Lin Zhang, Jiayou Hou, Tengjiao Xu, Bowen Song, Xi Bai, Hai Fu* and Peipei Guo*

Institute of Chemistry and Life science, Changchun University of Technology, Changchun, Jilin, 130012, P. R. China.

Table of Contents

1. Experimental section (page 2-3)

2. Crystal data of **H-1** and **H-2** (page 4)

3. Optimization conditions of the electrochemical synthesis **H-1e** (page 4)

4. Optimization conditions of the aerobic oxidation reaction by **H-1e** (page 5)

5. Comparison of benzyl alcohol oxidation on different MOF-based cataly (page 5)

6. Solvent accessible areas calculation by PLATON (page 5)

7. SEM of **H-1e** grown on Cu foil (page 6)

8. UV-visible spectra of methylene blue solution in methanol before and after adsorption (page 6)

9. FESEM-EDX of **H-1e** (page 7)

10. Fourier-Transform Infrared Spectra (FT-IR) of H_4L and **H-1** (page 7)

11. TGA of **H-1**, **H-1e** and **H-2**, FT-IR of **H-1e** after 4 recycles (page 7)

12. Raman spectra obtained from bare quartz container pristine (page 8)

13. Size selective effect of **H-1e**. (page 9)

14. N_2 gas sorption isotherms for **H-1e** (page 9)

15. Methanol oxygen in the anion of phenylcarbinol coordinated and oxidized with the catalyst **H-1**. (page 10)

16. Electronic cloud distribution and MO (page 10)

17. Energy barriers of different alcohols on the catalyst **H-1e** (page 11)

18. The SEM, TEM image and the EDS mapping of **H-1e** (page 12)

19. Two channels 1 and 2 in the asymmetric unit cell of **H-1e** (page 12)

20. Cartesian coordinates used for DFT Study (page 13 - page 16)

21. References (page 17 - page 18)

22. Copies of ^{1}H NMR and ^{13}C NMR Spectra (page 19 - page 29)

1 Experimental section

Synthesis of ligand H_4L

Ethyl 4-hydroxybenzoate (5.7 g, 35 mmol), Pentaerythrityl Tetrabromide (2.5 g, 6.5mmol) and K_2CO_3 (25 g, 0.18 mol) were poured into a round-bottom flask with 100 mL DMF, and refluxed at 120 °C for three days. The crudes were purified by silica column with the eluent ethyl acetate/petroleum ether (1:5). After the purification, the products were dissolved in 20 ml THF, then 10 ml MeOH and 8ml NaOH (4 M) were added. The yellowish solids were obtained by refluxing overnight under magnetic stirring at 50 °C.[1] Dilute hydrochloric acid was added dropwise until the solids dissolved, washed with deionized water for 3 times, then dried in vacuum to obtain the pure organic ligand namely H_4L (4,4'-((2,2-bis((4-carboxyphenoxy) methyl) propane-1,3-diyl) bis(oxy)) dibenzoic acid). The pure product of ligand H_4L was obtained as off-white solid in a yield of 76% based on Pentaerythrityl Tetrabromide.

Synthesis of ligand TPOM

4-hydroxypyridine (3.4 g, 36 mmol), Pentaerythrityl Tetrabromide (2.5 g, 6.5 mmol), K_2CO_3 (25 g, 0.18 mol) were poured into a round-bottom flask with 100 mL DMF, and refluxed under magnetic agitation condition for 3 days at 120 ℃. After cooling down to room temperature, the mixture was poured into ice water (3000 ml), producing white precipitates.[2] The crudes were dried in vacuum after extraction and filtration, and purified using silica column with MeOH/CH_2Cl_2 (1:5) as the eluent. The pure organic ligand TPOM (tetrakis (4-pyridyloxy-methylene) methane) dipyridine was obtained as off-white solid in a yield of 82% based on Pentaerythrityl Tetrabromide.

Synthesis of the compound H-1 ($C_{66}H_{56}Cu_4O_{28}$,12(O),4[DMF]) and H-2 ($C_{25}H_{24}Cu_4Cl_4N_4O_4$).

For **H-1**, A mixture of $Cu(NO_3)_2 \cdot 3H_2O$ (150 mg, 0.62 mmol), H_4L (50 mg, 0.08 mmol), H_2O/DMF = 3/7 (H_2O = 3.0 ml, DMF = 7.0 ml) was vigorously stirred for 30 min at room temperature. After stirring, the final pH value was adjusted to 6 with 1M HCl aq, then sealed in a glass autoclave reactor (15 mL), kept under 110 °C for 36 h. After cooling to room temperature at the rate of 10 °C/h, blue transparent block-shaped crystal samples of **H-1** were obtained, washed with ethanol for three times, and dried at room temperature. Transparent crystal samples of **H-1** were collected in 72% yields based on Cu. Anal. Calcd for $C_{66}H_{56}Cu_4O_{28}$,12(O),4[DMF]: C 45.41, H 3.21%; found: C 43.52, H 3.95%.

For **H-2**, A mixture of $Cu(NO_3)_2 \cdot 3H_2O$ (100 mg, 0.135 mmol), TPOM (60 mg, 0.135 mmol), H_2O/DMF = 4/6 (H_2O=3.0 ml, DMF=7.0 ml) was vigorously stirred for 30 min at room temperature. The final pH value was adjusted to 6 with 1M HCl, then sealed in a glass autoclave reactor (15 mL), kept under 105 °C for 24 h. After cooling to room temperature at the rate of 10 °C/h, blue transparent block-shaped crystal samples of **H-2** were received, washed with DMF for three times, and dried at room temperature. Transparent crystals of **H-2** were collected in 75% yields based on Cu. Calcd for $C_{25}H_{24}Cu_4Cl_4N_4O_4$: C 35.62, H 2.85, N 6.65%; found: C 36.23, H 2. 31, N 6.88%.

Synthesis of H-1e

The whole electrosynthesis process was carried out in a typical single cell (50 mL) with a two-electrode system comprising Cu foam sheets (1 × 1 cm^2) both as anode bathing

and cathode in a solution containing DMF/H_2O (7:3 v/v; 40 mL), $EmimBF_4$ (1.0 mL) and 2M HCl (1 ml) as supporting electrolyte. A small amount of organic ligand H_4L (nearly 80 mg, 0.12 mmol) was then dissolved in the above electrolyte solution under the condition of stirring, forming a homogeneous solution for 10 min under 6.0 V at 50 °C. Subsequently, blue precipitate was rapidly formed, collected by filtration, then washed with H_2O and DMF three times, dried in a vacuum. The material electrochemically synthesised is named **H-1e** throughout this paper. The pure product **H-1e** (blue crystal samples) was yield of 96% based on ligand H_4L. Since hydrochloric acid (HCl) was added in solvothermal synthesis to regulate acidity, to keep the same crystal structure, a small amount of hydrochloric acid was also used in electrochemical synthesis to regulate acidity. Meanwhile, HCl added in electrochemical synthesis could also form ions in the electrolyte and increase the conductivity of the solution a little.

2.Crystal data compounds of H-1 and H-2

Table S1.

Crystal data and structure refinements[3]

Compounds	**H-1**	**H-2**
formula	$C_{66}H_{56}Cu_4O_{28}$, 12(O), 4[DMF]	$C_{25}H_{24}Cl_4Cu_4N_4O_4$
formula weight	2035.72	840.486
T/K	293(2)	293(2)
wavelength (Å)	0.71073	0.71073
crystal system	'orthorhombic'	'tetragonal'
space group	*P*nna	*I*-4
a (Å)	27.857(3)	12.1241(9)
b (Å)	17.9648(17)	12.1241(9)
c (Å)	10.3908(10)	10.3617(14)
α/°	90	90
β/°	90	90
γ/°	90	90
V (Å^3)	5200.1(9)	1523.1(3)
Z	2	2
Dcalc (mg m^{-3})	1.300	1.833
μ /mm^{-1}	0.891	5.509
F(000)	2100.223	840.271
θ range (deg)	6.316 to 24.733	11.40 to 24.97
Rint	0.0533	0.0806
data/restraints/params	4372/0/251	1184/0/93
GOF on F^2	1.0629	1.0473
R_1[a], wR_2[b] (I>2σ(I))	0.0604	0.0554
R_1[a], wR_2[b] (all data)	0.0686	0.0612

[a]$R_1 = \Sigma||F_o|-|F_c||\Sigma/|F_o|$; [b]w$R_2 = \Sigma[w(F_o^2 - F_c^2)^2]/ \Sigma[w (F_o^2)^2]^{1/2}$

3. Optimization conditions of the electrochemical synthesis H-1e

Table S2.

Summary of synthesis parameters employed for synthesis of electrochemical **H-1e** samples

Sample	Voltage [V]	Reaction temperature[a]	Reaction time	Yield [%]
1	0 V	50 °C	1 h	0
2	2 V	30 °C	30 min	15
3	4 V	30 °C	30 min	37
4	6 V	30 °C	30 min	78
5	2 V	50 °C	30 min	33
6	4 V	50 °C	30 min	80
7	6 V	50 °C	20 min	96

[a]Reaction temperature, bath temperature of electrolyzer.

Table S3.

Optimization conditions of the aerobic oxidation reaction by **H-1e**

Entry	Solvent	T [℃]	Base	Yield [%]
1	CH_3CN	75	K_2CO_3	＞99
2	CH_3CN	75	KOH	91
3	CH_3CN	75	Na_2CO_3	96
4	CH_3CN	75	K_3PO_4	90
5	THF	75	K_2CO_3	88
6	Dioxane	75	K_2CO_3	81
7	DMF	75	K_2CO_3	53
8	CH_3CN	25	K_2CO_3	23
9	THF	25	K_2CO_3	18
10	Dioxane	25	K_2CO_3	20
11	DMF	25	K_2CO_3	15

Reaction conditions: benzyl alcohol (1 mmol); **H-1e** (10 mol%); TEMPO (0.5 equiv); K_2CO_3 (1 equiv); 10 mL solvent; 1 atm air; 75 ℃; 8 h.

Table S4.

Comparison of benzyl alcohol oxidation on different MOF-based catalysts.

Entry	Catalyst	Condition	Conv. [%]	Sel. [%]	Refs.
1	Cu-BTC	10 h, 95 °C, open air	23.9	99	4
2	$Cu_3(BTC)_2$	TEMPO, Na_2CO_3, 22 h, 75 °C, oxygen atmosphere	89		5
3	Cu-FMOF	TEMPO, Na_2CO_3, 16 h, 75 °C, air	94		6
4	$Cu(IMepyO)_2$ $Cu(IDippyO)_2$	TEMPO, KO^{t}Bu, 10 h, open air	81 99		7
5	$[(\eta^5\text{-}C_5Me_4{}^t\text{Bu})Ru(CO)(\mu\text{-}CO)]_2$	TEMPO, 6 h, open air	83		8
6	UiO-66	7 h, 130 °C, oxygen atmosphere	70		9
7	$[CuLCl_2]$	TEMPO, K_2CO_3, 40 °C, 1 atm air, 24 h	92	100	10
8	**H-1** **H-1e**	TEMPO, K_2CO_3, 75 °C, air, 8h	96 99	99 99	This work

Table S5.

Solvent accessible areas calculation by PLATON.

Area	Vol. Perc. (%)	Vol (Å^3)	X (av)	Y (av)	Z (av)
1	24.5	1281	0.250	0.294	0.074
2	24.5	1281	-0.250	0.700	-0.163

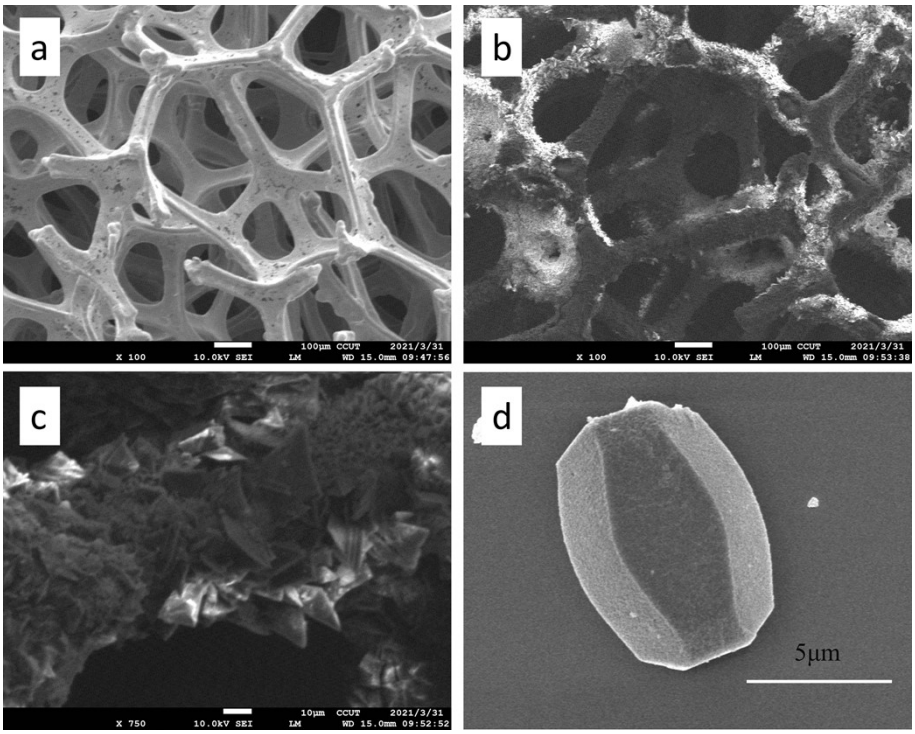

Fig. S1 SEM images of **H-1e** grown on Cu foil. (a) only Cu foil; (b, c) surface of Cu foil after electrolysis for 20 min; (d) sediment collected on the surface of Cu foil after electrolysis.

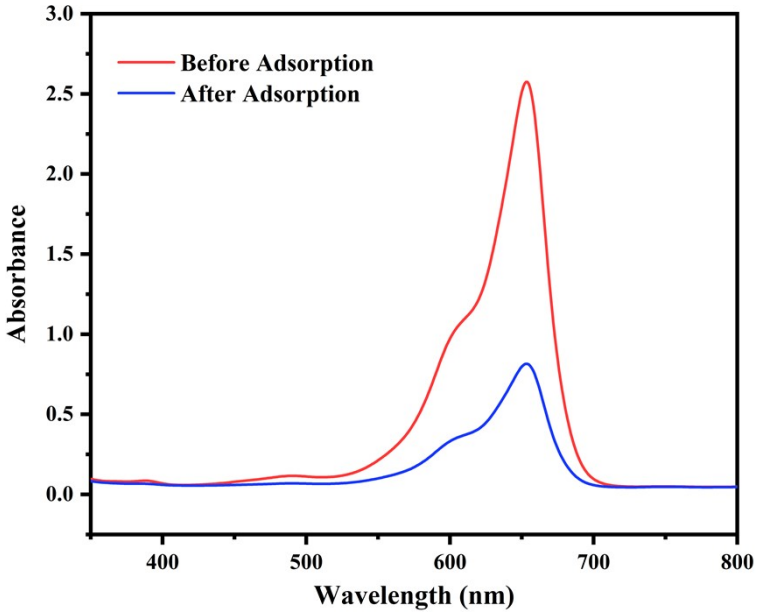

Fig. S2 UV-visible spectra of methylene blue solution in methanol before and after adsorption.

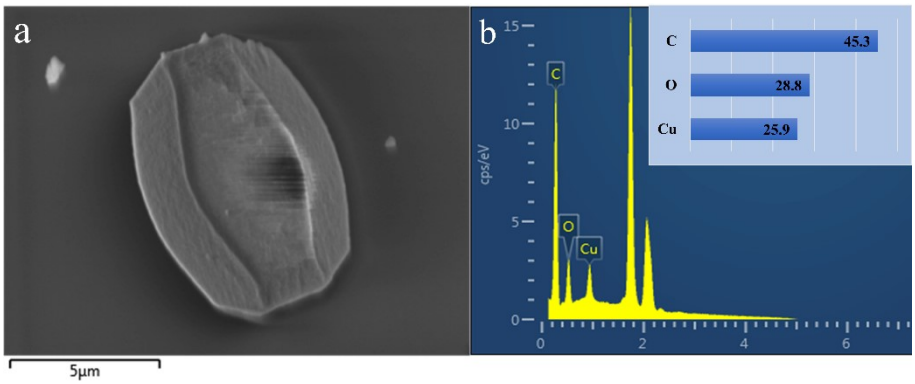

Fig. S3 FESEM-EDX of **H-1e**.

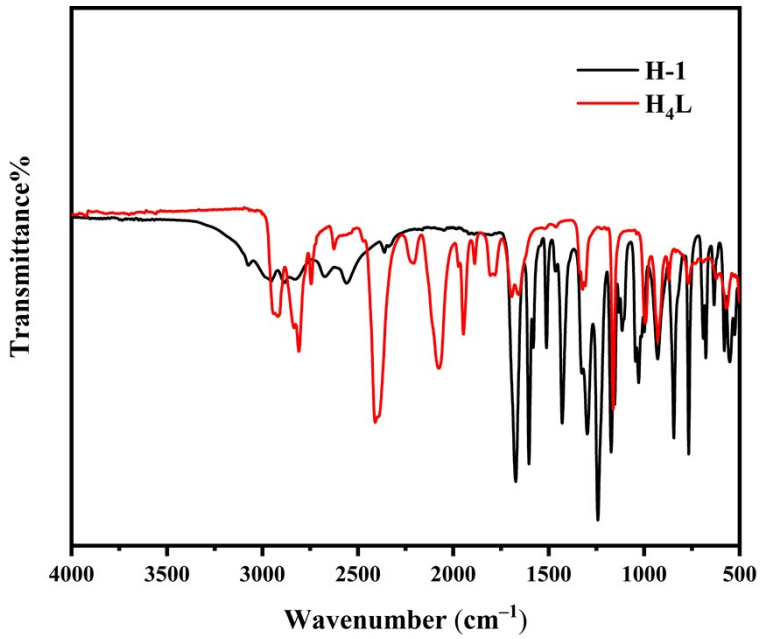

Fig. S4 Fourier-Transform Infrared Spectra (FT-IR) of organic ligand H_4L and **H-1**.

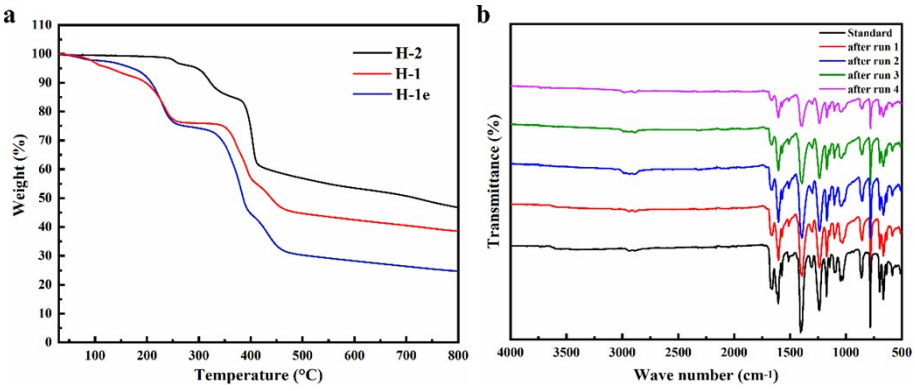

Fig. S5 (a) Thermogravimetric analysis (TGA) of **H-1**, **H-1e and H-2**; (b) Fourier-Transform Infrared Spectra (FT-IR) of **H-1e**; the standard data and the data after 4 recycles of **H-1e** in the oxidation of alcohols.

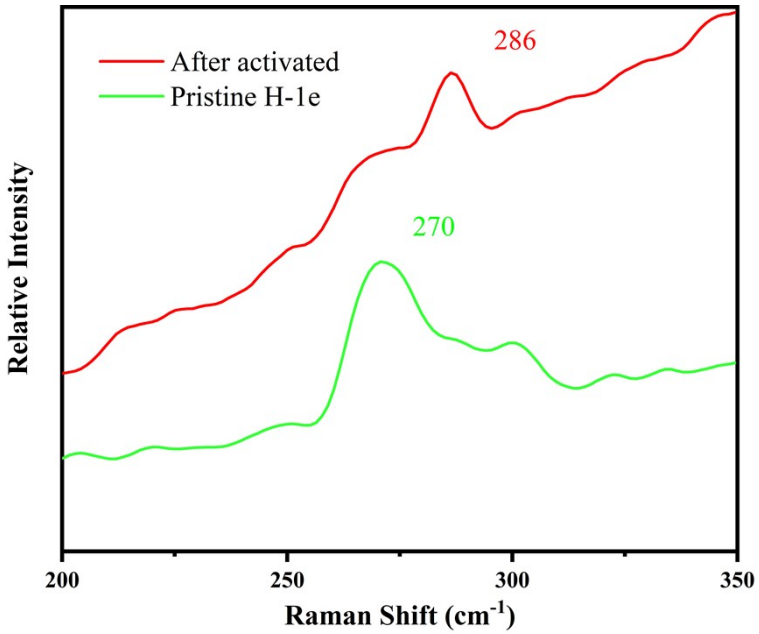

Fig. S6 Raman spectra (200-350 cm^{-1}) obtained from bare quartz container pristine (green curve) and activated (red curve) **H-1e**.

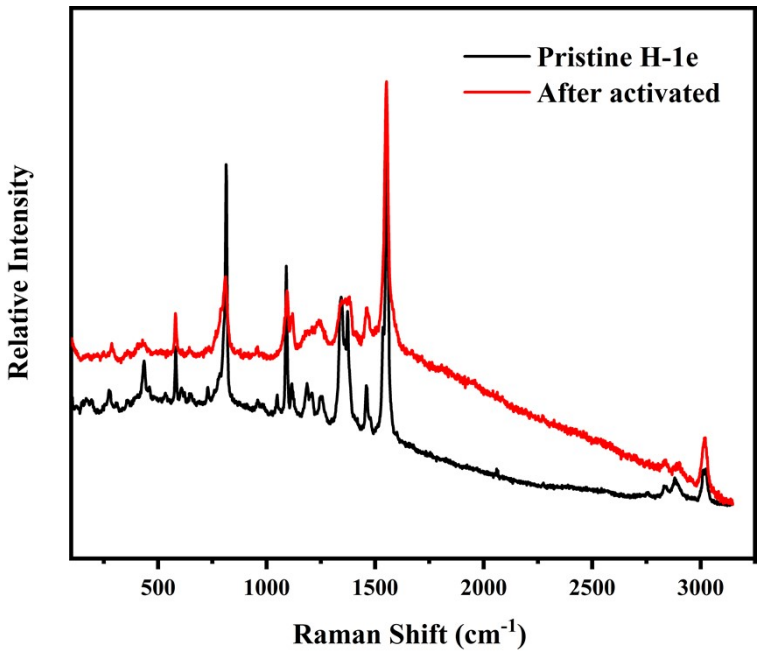

Fig. S7 Raman spectra (100-3250 cm^{-1}) obtained from bare quartz container pristine and activated **H-1e**.

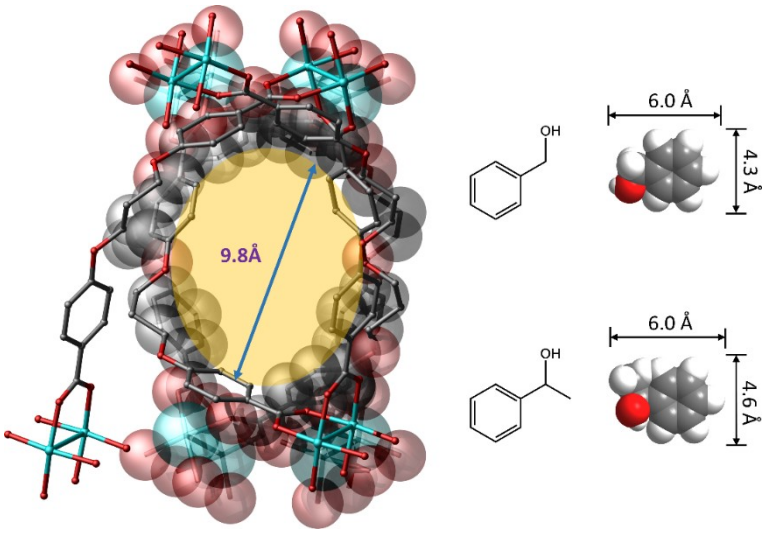

Fig. S8 Size selective effect of **H-1e**.

The channel size was estimated from the single-crystal structure by measuring the closest distance, and the effective pore size might be different from the estimation.

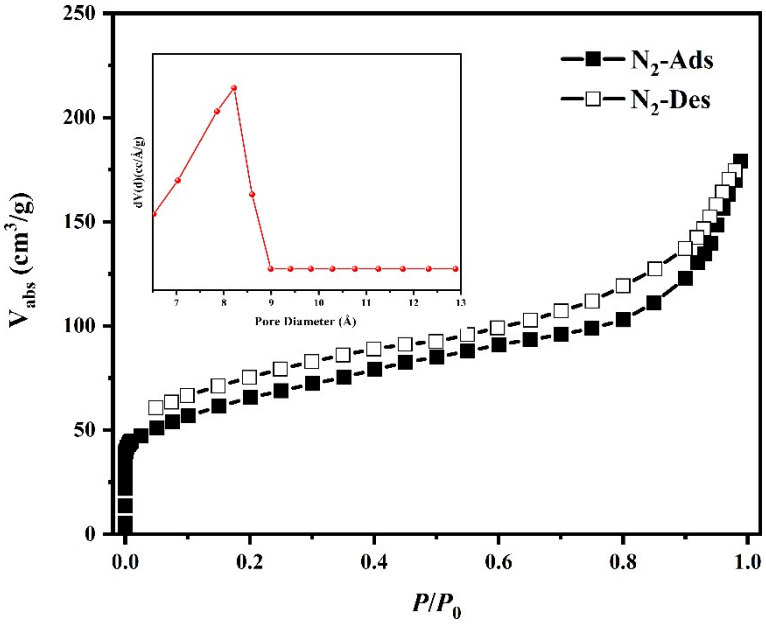

Fig. S9 N_2 sorption isotherms for **H-1e** at 77 K (inset: pore size distribution calculated by NLDFT method).

To investigate the permanent porosity of **H-1e**, N_2 adsorption experiments were performed. The crystalline materials were fully activated before the gas adsorption measurement. The crystals of **H-1e** were immersed in acetone three times for 12 h each, washed with methylene dichloride and then dried at room temperature to remove the guest solvents (DMF and H_2O). The samples were pretreated by degassing for 10 h at 100 °C under dynamic vacuum prior to the measurements. N_2 sorption isotherm is of classical type I behavior, characteristic of microporous materials, confirming the permanent porosity of the activated **H-1e**. There is a small hysteresis between adsorption and desorption isotherms, probably due to the retaining of N_2 in the flexible small channels or pore opening comparable to the size of N_2 molecule.

Calculated from the nitrogen adsorption data, the Langmuir surface area of **H-1e** is 607 m^2 g^{-1}. The pore size distributions calculated by the nonlocal density functional theory (NLDFT) method afforded a dominant peak at 0.83 nm. The result is a little smaller than the solvent-accessible surface area estimated based on the crystal structure. The discrepancy indicates the incomplete removal of guest molecules or structural deformation during the thermal activation of **H-1e**, which is often observed in MOFs.[11]

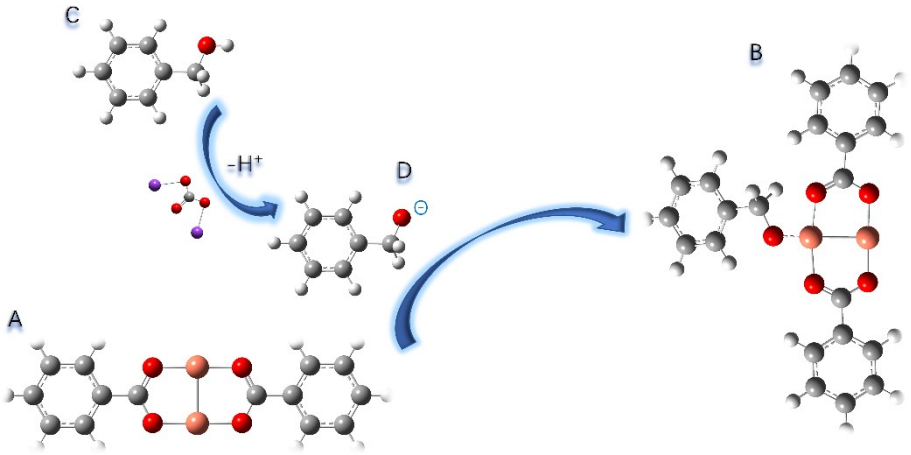

Fig. S10 Process of methanol oxygen in the anion of phenylcarbinol coordinated and oxidized with the copper center in the activated catalyst **H-1**. O(ne-)-Cu(dp) interaction energy for Cu coordinated transition state of activated catalyst **H-1** with phenylcarbinol. Free energy calculation of transition state ΔG(A-B) = -124.5 Kcal/mol. *G* (kcal/mol) using M06/6-31G(d)/auto geometry optimizations followed by M06/6-311+G(2d,p)/SDD single point including SMD/acetonitrile. Orange = Cu, Red = O, grey = C, purple = K, and light grey = H.

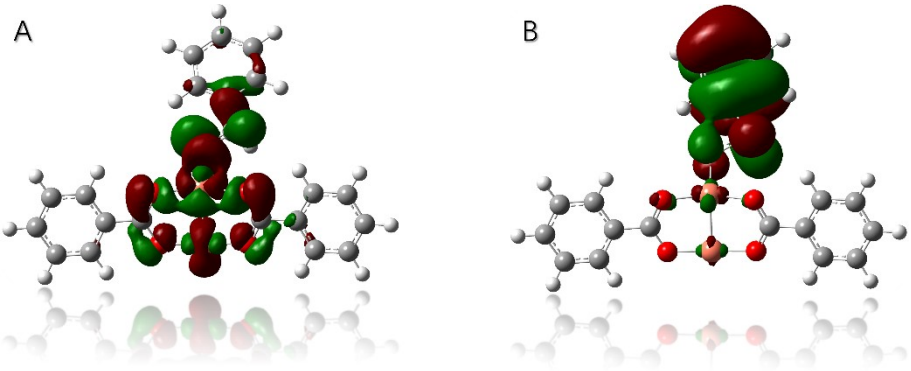

Fig. S11 Alpha MO (left) and beta MO (right) of transition state with oxygen coordinated to copper center in activated catalyst **H-1**.

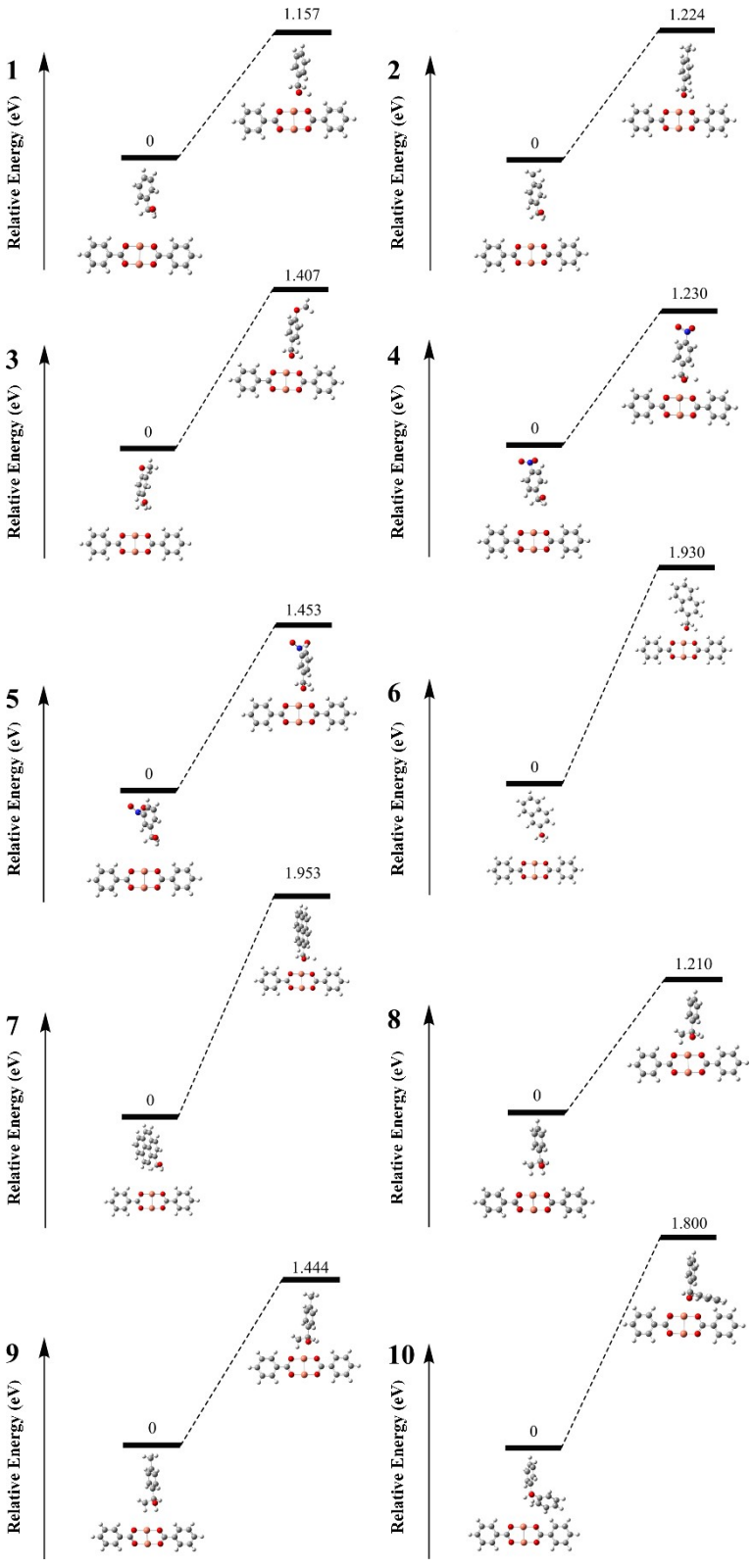

Fig. S12 Energy barriers of different alcohols on the catalyst **H-1e**.

The first step of oxidation occurs, when one hydrogen was dissociated from the hydroxyl group on the alcohol under the existence of the active OCSs in **H-1e**. This process needs to overcome the energy barrier. As **Fig. S12** shown, it is found that the substrate with smaller molecular size shows lower energy barrier, and is prone to react dynamically. However, the larger substrate

shows higher energy barrier, and is not easy to react. It is consistent with our catalytic experimental results well.[12-13] It is also accept that pore size (and hence mass transport) and steric hindrance show an influence on the catalytic activity of different substrate.[14]

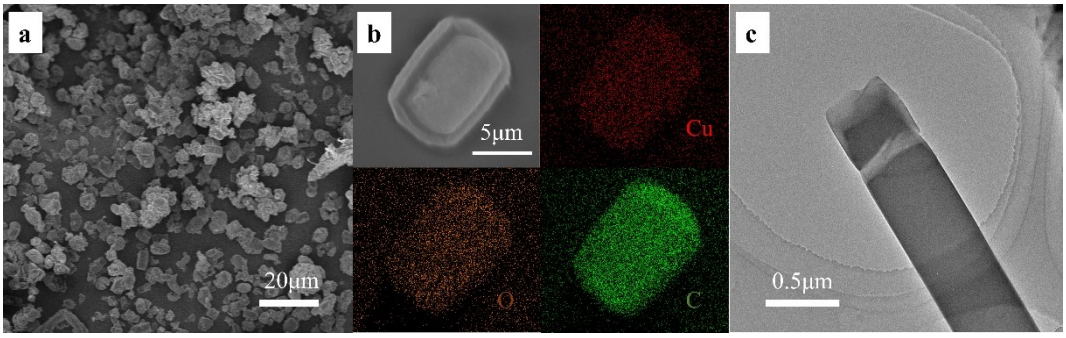

Fig. S13 (a) SEM image, (b) EDX mappings and (c) the TEM image of **H-1e** samples after 4 recycles.

The SEM image and the EDS mapping of **H-1e** the catalyst after stability test were taken to further characterize **H-1e** after 4 recycles. As the SEM images before and after the stability test shown, there is no obvious change among the catalyst samples **H-1e**.

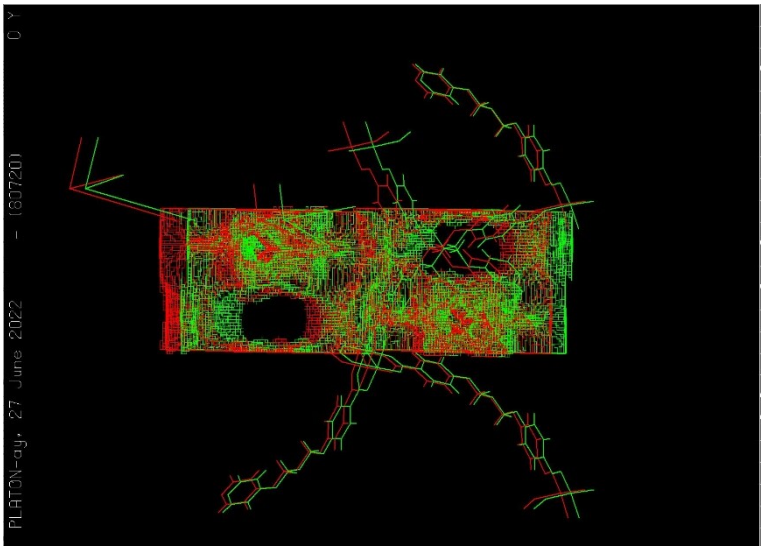

Fig. S14 Two channels 1 and 2 in the asymmetric unit cell of **H-1e** (view along *y*-axis).

To further characterized the position of the pores in the asymmetric unit cell of **H-1e**, software PLATON was introduced to calculate the pores. As the **Fig. S14** and **Table S5** shown, there are two channels 1 and 2 in the asymmetric unit cell. The volume of each pore is about 1281 Å^3 with 24.5% in total volume of the unit cell. The coordinates (X, Y, Z) of the two channels are 0.250, 0.294, 0.074 and -0.250, 0.700, -0.163 (av), respectively.

Cartesian coordinates used for DFT Study:

The structures of all compounds were optimized using *Gaussian09* Revision A.02 using the M06L density functional and LANL2DZ basis set and effective core potential with the automatically generated density fitting functions.[15-18] Minima and transition states were confirmed by vibrational frequency calculations. Single point calculations were performed using the M06-2X functional and the 6-311+G (2d,p) basis set on nonmetal atoms and SDD basis set and effective core potential for copper.[19-23] To account for solvent effects, the SMD implicit solvent model with acetonitrile was used in these single point calculations.[24]

Cartesian coordinates for all structures and gas phase Gibbs energy and Gibbs energy including solvation correction are listed below. [To obtain the Gibbs free energy with relevant standard state reference, G^{o} (298K, 1M) = G^{o*}(298K, 1 atm) + RT ln(0.08206T), where R is the gas constant and T is the temperature. ΔG_0(298K, 1 M) = ΔG_0^*(298K, 1 atm) when there is no mole change from the reactant to the product.[25]

Energy is from M06/6-311g (2d,p)/SDD/SMD(acetonitrile) single points. Gibbs Energy uses this energy and the Gibbs energy correction from the optimization and frequency calculations with M06l/LANL2DZ. All energies are in Hartrees. Grey spheres represent carbon, light grey for hydrogen, red for oxygen, purple for potassium, and yellow for copper.

a. Cartesian coordinates used for phenylmethanol

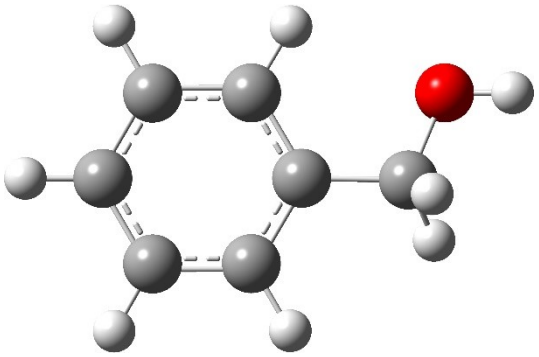

E = -346.601330566 Hartrees

G = -346.500601566 Hartrees

C	1.86358485	1.01591594	-0.08506814
C	0.49802008	1.29556494	-0.02409142
C	-0.43900678	0.26120826	0.08124877
C	0.01270748	-1.06252709	0.11256938
C	1.37792069	-1.34401972	0.04222704
C	2.30797142	-0.30718475	-0.05258383
H	2.57865930	1.83037375	-0.16759745
H	0.15693997	2.32843212	-0.06205862
H	-0.71388858	-1.86541270	0.17849364
H	1.71578443	-2.37707610	0.06191856
H	3.37067795	-0.52813180	-0.10722912
C	-1.91139310	0.58279658	0.20507984
H	-2.15660759	0.76358244	1.26604439
H	-2.12856016	1.51855939	-0.33522028
O	-2.68412923	-0.49811934	-0.30543894

H	-3.60879935	-0.33589735	-0.06712940

b. Cartesian coordinates used for K_2CO_3

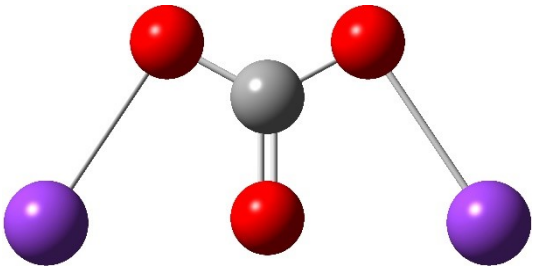

E = -1463.68424650 Hartrees

G = -1,463.7006045 Hartrees

C	-0.00029261	0.80129415	0.00003953
O	1.12756730	1.41271108	0.00070022
O	-1.12794076	1.41302839	-0.00072409
O	-0.00041560	-0.54970721	0.00012089
K	2.48481023	-0.60556248	-0.00016276
K	-2.48438559	-0.60580715	0.00010943

c. Cartesian coordinates used for **H-1**

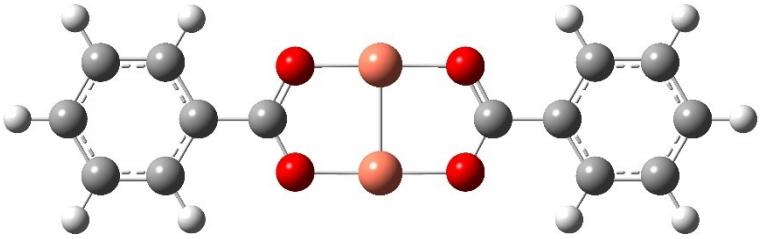

E = -4120.97407473 Hartrees

G = -4120.81074173 Hartrees

Cu	-0.00000495	-1.15371096	0.00067952
Cu	-0.00000492	1.15370885	-0.00078329
O	1.82624149	-1.13246694	-0.00059913
O	1.82624005	1.13246797	0.00058302
O	-1.82625932	-1.13247134	0.00130203
O	-1.82625673	1.13245070	-0.00130044
C	3.90115149	0.00000204	0.00001915
C	4.60739734	-1.21159760	-0.00051812
C	4.60739643	1.21160092	0.00057520
C	5.99998554	-1.21034388	-0.00049768
H	4.05098483	-2.14212781	-0.00094714
C	5.99998580	1.21034812	0.00059193
H	4.05098506	2.14213198	0.00098804
C	6.69810871	0.00000272	0.00005665
H	6.54160655	-2.15216956	-0.00091516
H	6.54160496	2.15217491	0.00102301
H	7.78497459	0.00000197	0.00007069
C	-3.90112791	-0.00000537	0.00002252

C	-4.60737232	1.21159185	0.00085815
C	-4.60738686	-1.21159266	-0.00079901
C	-5.99996479	1.21035041	0.00091823
H	-4.05096406	2.14212440	0.00144910
C	-5.99998062	-1.21033245	-0.00082961
H	-4.05099629	-2.14213572	-0.00140236
C	-6.69810156	0.00001286	0.00005162
H	-6.54156951	2.15218519	0.00162597
H	-6.54159565	-2.15216122	-0.00152622
H	-7.78496803	0.00002064	0.00006273
C	-2.41794099	-0.00000927	0.00000372
C	2.41793306	0.00000119	-0.00000329

d. Cartesian coordinates used for intermediate

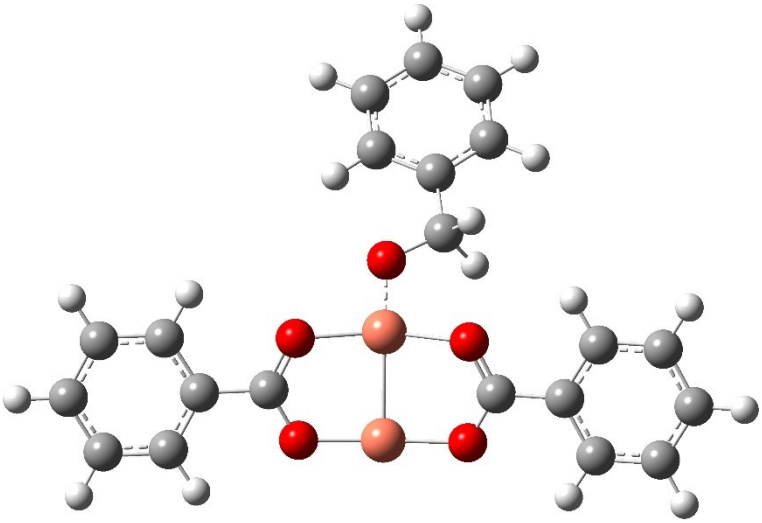

E = -4466.73884285 Hartrees

G = -4466.46534685 Hartrees

Cu	-0.00000677	-1.77371066	0.00128950
O	1.82623968	-1.75246664	0.00001086
O	1.82623823	0.51246827	0.00119300
O	-1.82626114	-1.75247104	0.00191202
O	-1.82625854	0.51245100	-0.00069045
C	3.90114968	-0.61999766	0.00062913
C	4.60739552	-1.83159730	0.00009187
C	4.60739462	0.59160122	0.00118518
C	5.99998372	-1.83034358	0.00011230
H	4.05098301	-2.76212751	-0.00033716
C	5.99998399	0.59034842	0.00120191
H	4.05098324	1.52213228	0.00159802
C	6.69810689	-0.61999698	0.00066663
H	6.54160473	-2.77216925	-0.00030518
H	6.54160314	1.53217521	0.00163300
H	7.78497277	-0.61999773	0.00068067

C	-3.90112973	-0.62000507	0.00063250
C	-4.60737414	0.59159215	0.00146813
C	-4.60738867	-1.83159236	-0.00018903
C	-5.99996661	0.59035071	0.00152821
H	-4.05096587	1.52212470	0.00205908
C	-5.99998243	-1.83033215	-0.00021962
H	-4.05099811	-2.76213542	-0.00079238
C	-6.69810338	-0.61998684	0.00066160
H	-6.54157132	1.53218549	0.00223596
H	-6.54159746	-2.77216092	-0.00091624
H	-7.78496984	-0.61997906	0.00067271
C	-2.41794280	-0.62000897	0.00061371
C	2.41793125	-0.61999851	0.00060669
O	-0.00000029	2.73370809	-0.00233776
Cu	-0.00000673	0.53370915	-0.00017330
C	-1.34795413	3.21106321	0.00491050
H	-1.85645929	2.85684858	-0.86735924
H	-1.84861683	2.85246304	0.87992066
C	-1.34714890	4.75105815	0.00877216
C	-1.34671274	5.45170997	-1.19717502
C	-1.34646127	5.44559180	1.21907753
C	-1.34678764	6.84686532	-1.19357537
H	-1.34762471	4.90466132	-2.15110307
C	-1.34605712	6.84041239	1.22259849
H	-1.34674611	4.89293700	2.16979774
C	-1.34661678	7.54112832	0.01619609
H	-1.34689370	7.39907955	-2.14447088
H	-1.34550709	7.38807561	2.17629599
H	-1.34649588	8.64072819	0.01921624

References

1 T. Tu, T. Maris and J. D, Wuest, Synthesis and Structure of Spirocyclic Tetraethers Derived from [1,1′-Binaphthalene]-2,2′-diol and Pentaerythritol, *J. Org. Chem*., 2008, **73** (14), 5255-5263.

2 M. Baldrighi, P. Metrangolo, F. Meyer, T. Pilati, D. Proserpio, G. Resnati and G. Terraneo, Halogen-bonded and interpenetrated networks through the self-assembly of diiodoperfluoroarene and tetrapyridyl tectons, *J. Fluorine Chem.*, 2010, **131**, 1218-1224.

3 O. V. Dolomanov, L. J. Bourhis, R. J. Gildea, J.A.K. Howard and H. Puschmann, OLEX2: A complete structure solution, refinement and analysis program, *J. Appl. Cryst*.,2009, **42**, 339-341.

4 L. Peng, S. Wu, X. Yang, J. Hu, X. Fu, M. Li, L. Bai, Q. Huo and J. Guan, Oxidation of benzyl alcohol over metal organic frameworks M-BTC (M = Co, Cu, Fe), *New J. Chem.*, 2017, **41**, 2891-2894.

5 A. Dhakshinamoorthy, M. Alvaro and H. Garcia, Aerobic Oxidation of Benzylic Alcohols Catalyzed by Metal−Organic Frameworks Assisted by TEMPO, *ACS Catal.*, 2010, **1**, 48-53.

6 S. C. Chen, S. N. Lu, F. Tian, N. Li, H. Y. Qian, A.-J. Cui, M.-Y. He and Q. Chen, Highly selective aerobic oxidation of alcohols to aldehydes over a new Cu(II)-based metal-organic framework with mixed linkers, *Catal. Commun.*, 2017, **95**, 6-11.

7 I. Ahmad Bhat, I. Avinash, S. Kumar Sachan, S. Singh and G. Anantharaman, Efficient Synthesis of Cu(II)-N-Heterocyclic Carbene Complexes in Water and Their Activity Towards Aerobic Alcohol Oxidation, *Eur. J. Inorg. Chem.*, 2021, **2021**, 4560-4565.

8 Z. Hao, X. Yan, Z. Li, R. Wu, Z. Ma, S. Li, Z. Han, X. Zheng and J. Lin, Efficient aerobic oxidation of alcohols to aldehydes and ketones using a ruthenium carbonyl complex of a tert-butyl-substituted tetramethylcyclopentadienyl ligand as catalyst, *Transit. Metal. Chem.*, 2018, **43**, 635-640.

9 H. Ghasempour, F. ZareKarizi, A. Morsali and X.-W. Yan, Development of a highly porous Fe-based MOF using symmetrically incompatible building blocks: Selective oxidation of benzyl alcohols, *Appl. Mater. Today*, 2021, **24**, 101157.

10 A. Bocian, A. Gorczyński, D. Marcinkowski, S. Witomska, M. Kubicki, P. Mech, M. Bogunia, J. Brzeski, M. Makowski, P. Pawluć and V. Patroniak, New benzothiazole based copper(II) hydrazone Schiff base complexes for selective and environmentally friendly oxidation of benzylic alcohols: The importance of the bimetallic species tuned by the choice of the counterion, *J. Mol. Liq.*, 2020, **302**, 112590.

11 L. L. Liang, J. Zhang, S.-B. Ren, G. W. Ge, Y. Z. Li, H. B. Du and X. Z. You, Rational synthesis of a microporous metal–organic framework with PtS topology using a semi-rigid tetrahedral linker, CrystEngComm., 2010, 12, 2008-2010.

12 J. Goclon and K. Winkler, Influence of nitrogen vacancies on selective oxidation of aromatic alcohols on g-C3N4: A comparative DFT study, *Mol, Catal.*, 2020, **482,** 110747.

13 Z. Li, T. Fan, H. Li, X. Lu, S. Ji, J. Zhang, J. H. Horton, Q. Xu and J. Zhu, Atomically Defined Undercoordinated Copper Active Sites over Nitrogen-Doped Carbon for Aerobic Oxidation of Alcohols, *Small*, 2022, **18**, 2106614.

14 X. C. Kang, K. Lyu, L. L. Li, J. N. Li, L. Kimberley, B. Wang, L. F. Liu, Y. Q. Cheng, M. D. Frogley, S. Rudić, A. J. Ramirez-Cuesta, R. A.W. Dryfe, B. X. Han, S. H. Yang and M.

Schröder, Integration of mesopores and crystal defects in metal-organic frameworks via templated electrosynthesis, *Nat. Commun*., 2019, **10**, 4466.

15 M. J. Frisch, G. W. Trucks, H. B. Schlegel, G. E. Scuseria, M. A. Robb, J. R. Cheeseman, G. Scalmani, V. Barone, B. Mennucci, G. A. Petersson, H. Nakatsuji, M. Caricato, X. Li, H. P. Hratchian, A. F. Izmaylov, J. Bloino, G. Zheng, J. L. Sonnenberg, M. Hada, M. Ehara, K. Toyota, R. Fukuda, J. Hasegawa, M. Ishida, T. Nakajima, Y. Honda, O. Kitao, H. Nakai, T. Vreven, J. A. Montgomery, Jr., J. E. Peralta, F. Ogliaro, M. Bearpark, J. J. Heyd, E. Brothers, K. N. Kudin, V. N. Staroverov, R. Kobayashi, J. Normand, K. Raghavachari, A. Rendell, J. C. Burant, S. S. Iyengar, J. Tomasi, M. Cossi, N. Rega, J. M. Millam, M. Klene, J. E. Knox, J. B. Cross, V. Bakken, C. Adamo, J. Jaramillo, R. Gomperts, R. E. Stratmann, O. Yazyev, A. J. Austin, R. Cammi, C. Pomelli, J. W. Ochterski, R. L. Martin, K. Morokuma, V. G. Zakrzewski, G. A. Voth, P. Salvador, J. J. Dannenberg, S. Dapprich, A. D. Daniels, O. Farkas, J. B. Foresman, J. V. Ortiz, J. Cioslowski, and D. J. Fox, Gaussian, Inc., Wallingford CT, 2009.

16 Y. Zhao and D. G. Truhlar. A new local density functional for main-group thermochemistry, transition metal bonding, thermochemical kinetics, and noncovalent interactions, *J. Chem. Phys*., 2006, **125**, 194101, 1-18.

17 T. H. Dunning Jr. and P. J. Hay, in Modern Theoretical Chemistry, Ed. H. F. Schaefer III, Plenum, New York, 1977, **3**, S4, 1-28.

18 P. J. Hay and W. R. Wadt. Ab initio effective core potentials for molecular calculations potentials for the transition-metal atoms Sc to Hg, *J. Chem. Phys*., 1985, **82**, 270-283.

19 Y. Zhao and D. G. Truhlar, The M06 suite of density functionals for main group thermochemistry, thermochemical kinetics, noncovalent interactions, excited states, and transition elements: two new functionals and systematic testing of four M06-class functionals and 12 other functionals, *Theor. Chem. Acc*., 2008, **120**, 215-241.

20 A. D. McLean and G. S. Chandler, Contracted Gaussian-basis sets for molecular calculations. 1. 2nd row atoms, Z=11-18, *J. Chem. Phys*., 1980, **72**, 5639-5648.

21 K. Raghavachari, J. S. Binkley, R. Seeger, and J. A. Pople. Self-Consistent Molecular Orbital Methods. 20. Basis set for correlated wave-functions, *J. Chem. Phys*., 1980, **72**, 650-654.

22 H. Stoll, P. Fuentealba, P. Schwerdtfeger, J. Flad, L. v. Szentpály, and H. Preuss, Cu and Ag as one-valence-electron atoms - CI results and quadrupole corrections of Cu2, Ag2, CuH, and AgH, *J. Chem. Phys*., 1984, **81**, 2732-2736.

23 D. Andrae, U. Haeussermann, M. Dolg, H. Stoll, and H. Preuss, Energy-adjusted ab initio pseudopotentials for the 2nd and 3rd row transition-elements, *Theor. Chem. Acc*., 1990, **77**, 123-141.

24 A. V. Marenich, C. J. Cramer, and D. G. Truhlar, Universal solvation model based on solute electron density and a continuum model of the solvent defined by the bulk dielectric constant and atomic surface tensions, *J. Phys. Chem. B.*, 2009, **113,** 6378-6396.

25 P. K. Behera, P. Choudhury, S. K. Sahu, R. R. Sahu, A. N. Harvat, C. McNulty, A. Stitgen, J. Scanlon, M. Kar and L. Rout, Oxygen Bridged Bimetallic $CuMoO_4$ Nanocatalyst for Benzylic Alcohol Oxidation; Mechanism and DFT Study, *Asian J. Org. Chem.*, 2021, **10**, 1117-1122.

^{1}H NMR (400 MHz, DMSO-d_6) δ 12.62 (s, 4H), 7.86 (d, J = 7.7 Hz, 8H), 7.08 (d, J = 8.4 Hz, 8H), 4.39 (d, J = 7.0 Hz, 8H).

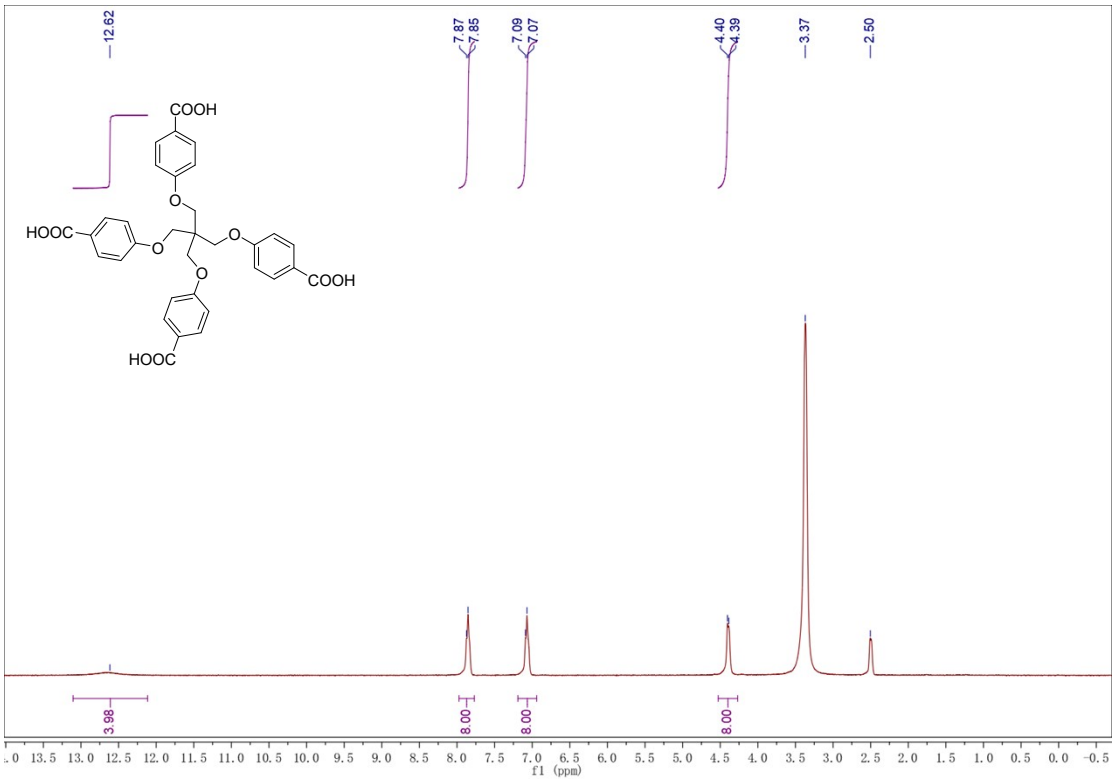

^{1}H NMR (400 MHz, DMSO-d_6) δ 12.62 (s, 4H), 7.86 (d, J = 7.7 Hz, 8H), 7.08 (d, J = 8.4 Hz, 8H), 4.39 (d, J = 7.0 Hz, 8H).

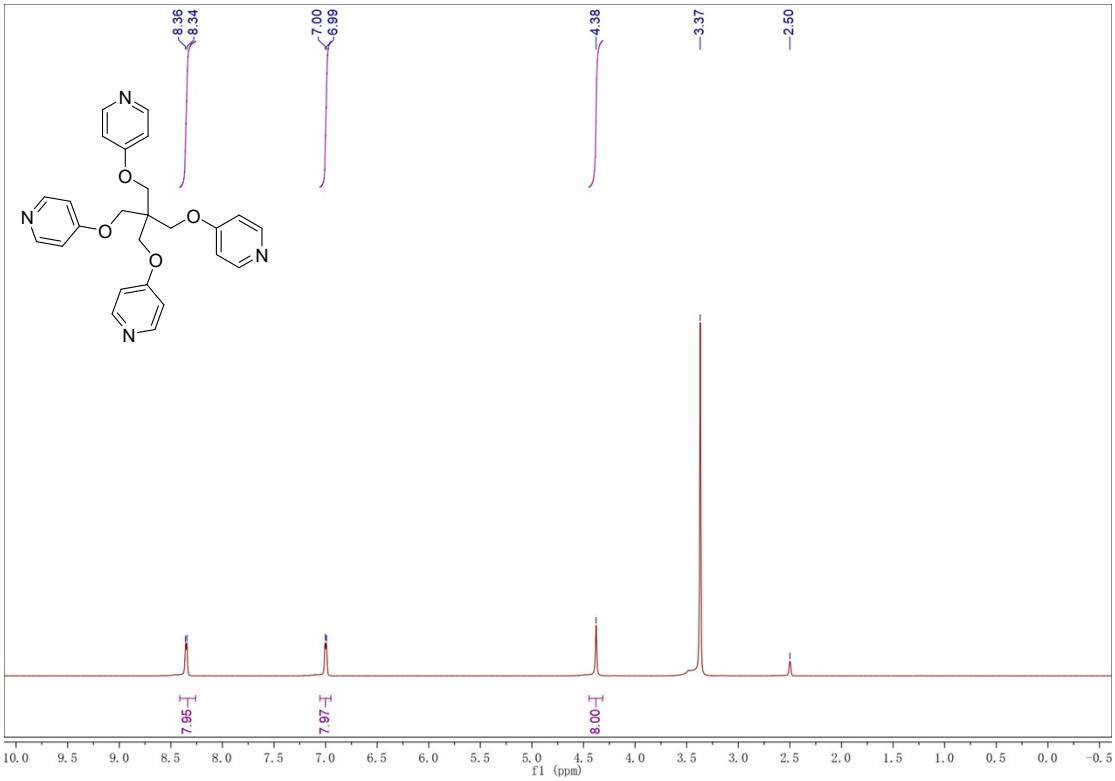

^{1}H NMR and ^{13}C NMR spectra

1. benzaldehyde：^{1}H NMR (400 MHz, DMSO-d_6) δ 10.02 (s, 1H), 7.94 – 7.88 (m, 2H), 7.71 (d, J = 8.1 Hz, 1H), 7.61 (t, J = 7.5 Hz, 2H). ^{13}C NMR (101 MHz, $CDCl_3$) δ 192.31, 136.45, 134.42, 129.71, 128.98.

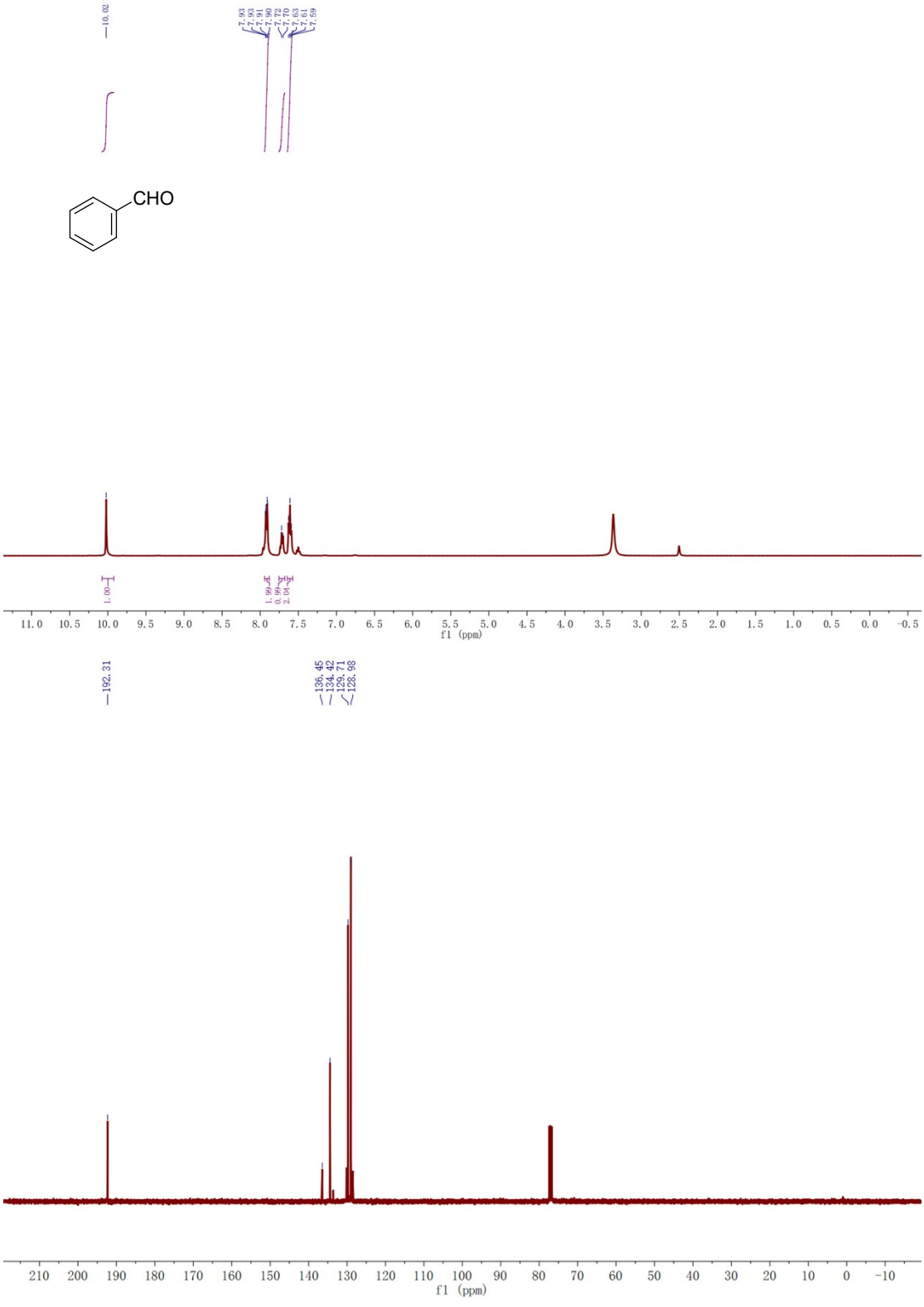

2. 4-methylbenzaldehyde：^{1}H NMR (400 MHz, Chloroform-d) δ 10.04 (s, 1H), 7.85 (d, J = 7.8 Hz, 2H), 7.41 (d, J = 7.6 Hz, 2H), 2.52 (s, 3H). ^{13}C NMR (101 MHz, CDCl3) δ 192.01, 145.56, 134.32, 129.91, 21.95.

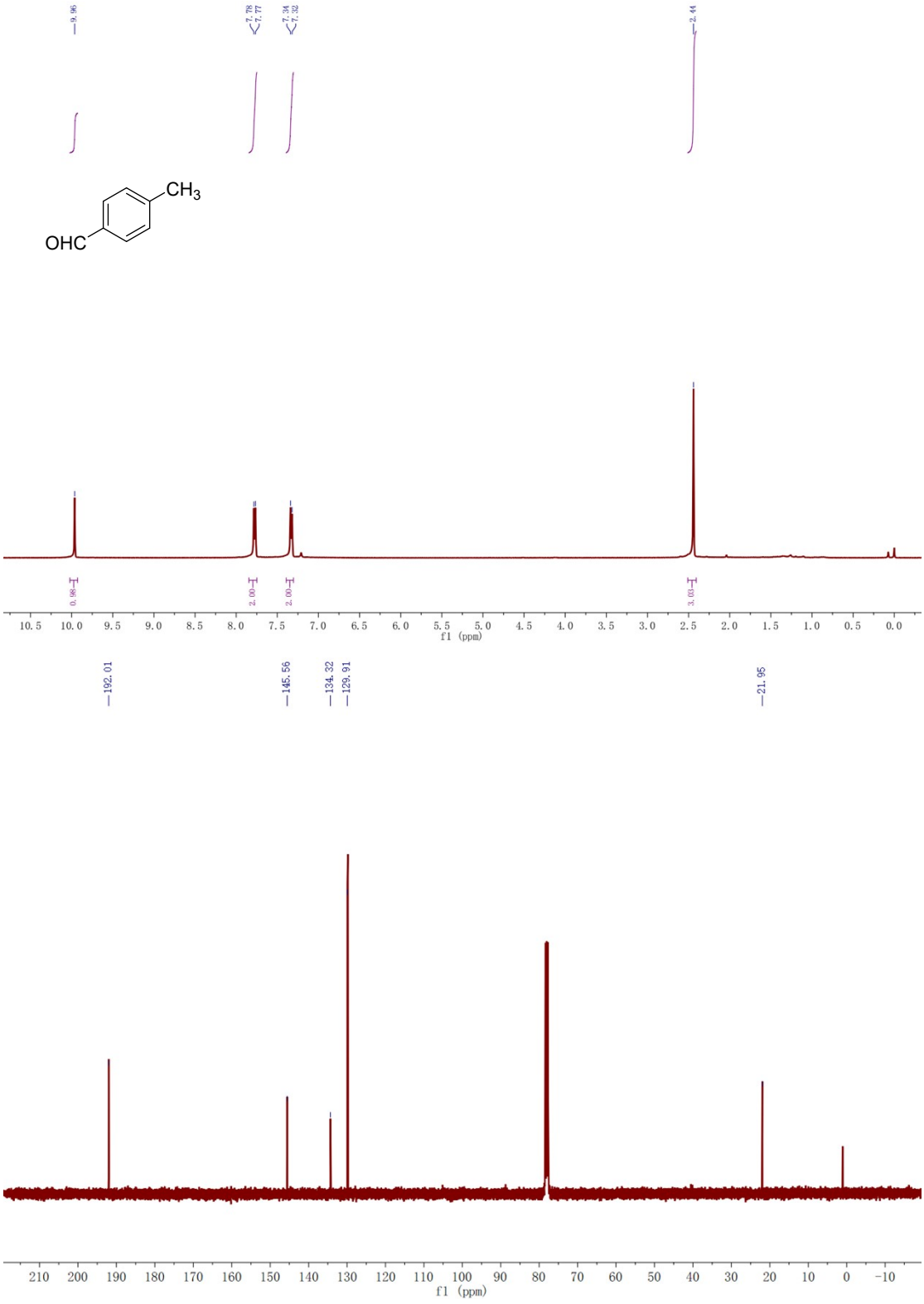

3. 4-methoxybenzaldehyde：^{1}H NMR (400 MHz, Chloroform-d) δ 9.88 (s, 1H), 7.84 (d, J = 7.9 Hz, 2H), 7.00 (d, J = 7.9 Hz, 2H), 3.89 (s, 3H). ^{13}C NMR (101 MHz, CDCl3) δ 190.76, 164.65, 131.99, 130.06, 114.37, 55.64.

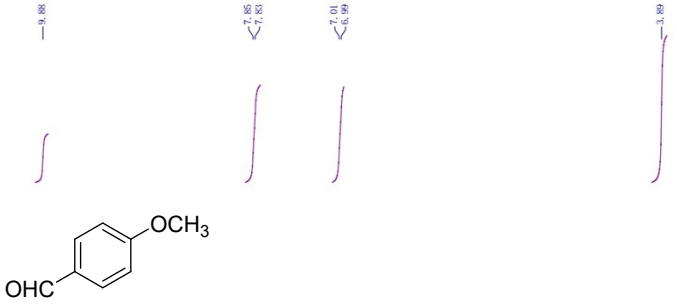

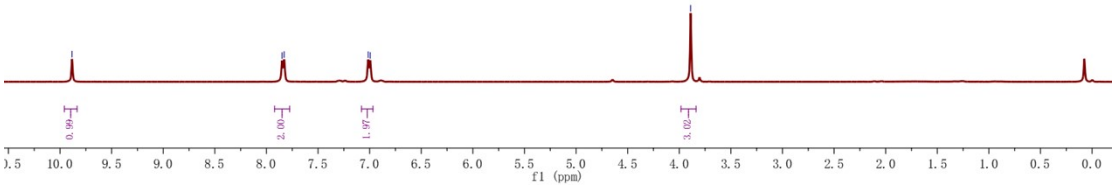

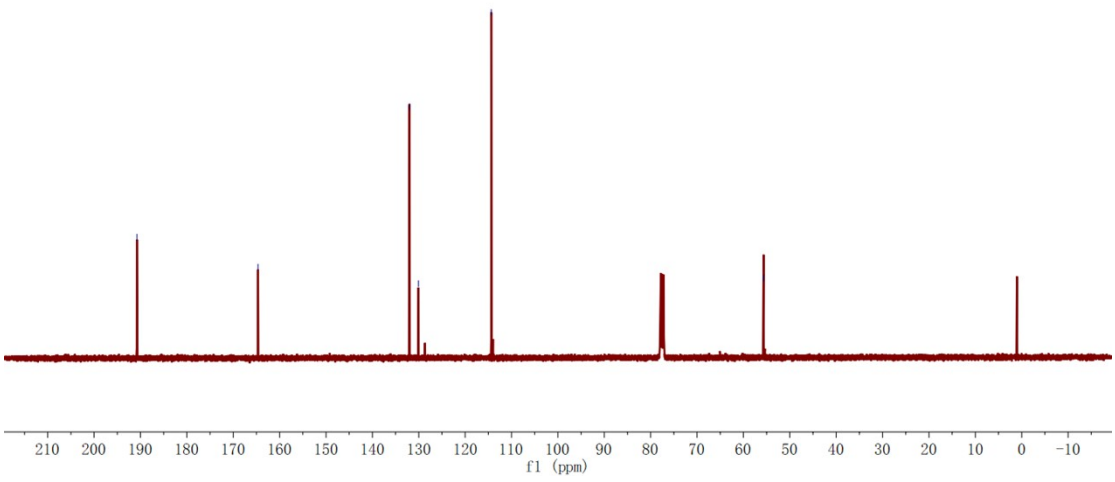

4. 4-nitrobenzaldehyde：^{1}H NMR (400 MHz, Chloroform-d) δ 10.16 (s, 1H), 8.39 (d, J = 8.4 Hz, 2H), 8.07 (d, J = 8.6 Hz, 2H).

^{13}C NMR (101 MHz, CDCl3) δ 190.14, 140.08, 130.44, 124.29, 99.98.

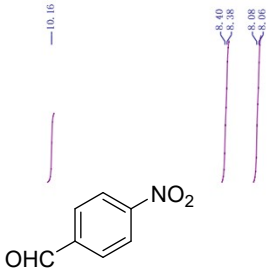

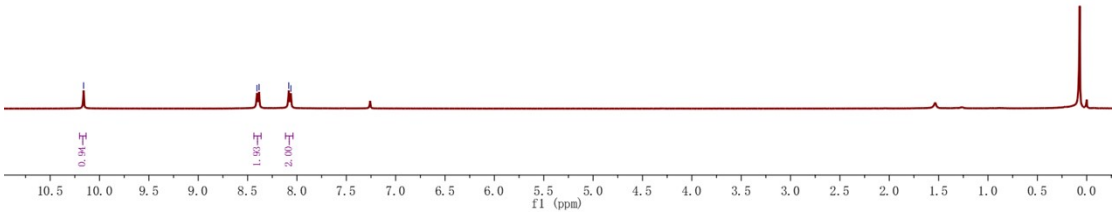

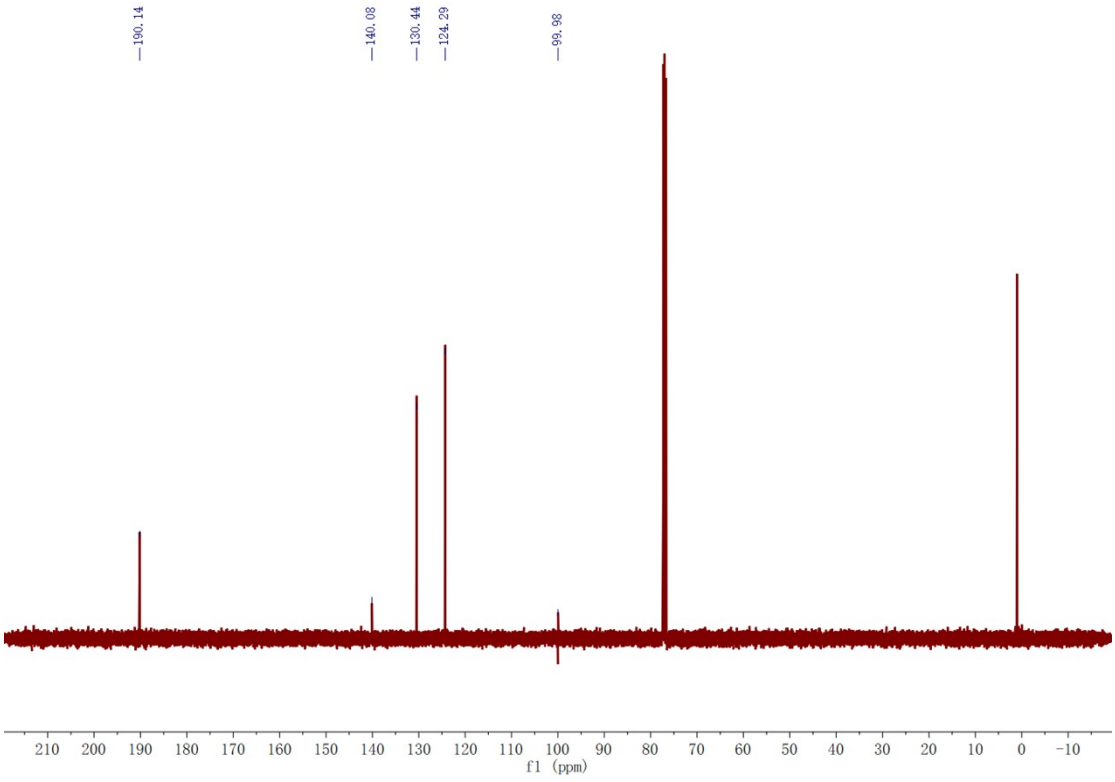

5. 3-nitrobenzaldehyde：^{1}H NMR (400 MHz, Chloroform-d) δ 10.13 (s, 1H), 8.72 (s, 1H), 8.50 (d, J = 7.4 Hz, 1H), 8.24 (d, J = 7.6 Hz, 1H), 7.78 (t, J = 7.9 Hz, 1H). ^{13}C NMR (101 MHz, CDCl3) δ 189.62, 137.45, 134.57, 130.36, 124.44.

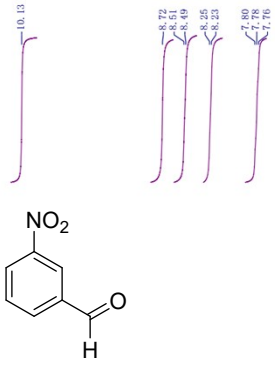

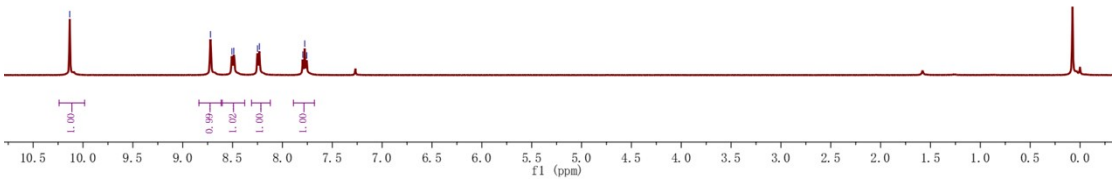

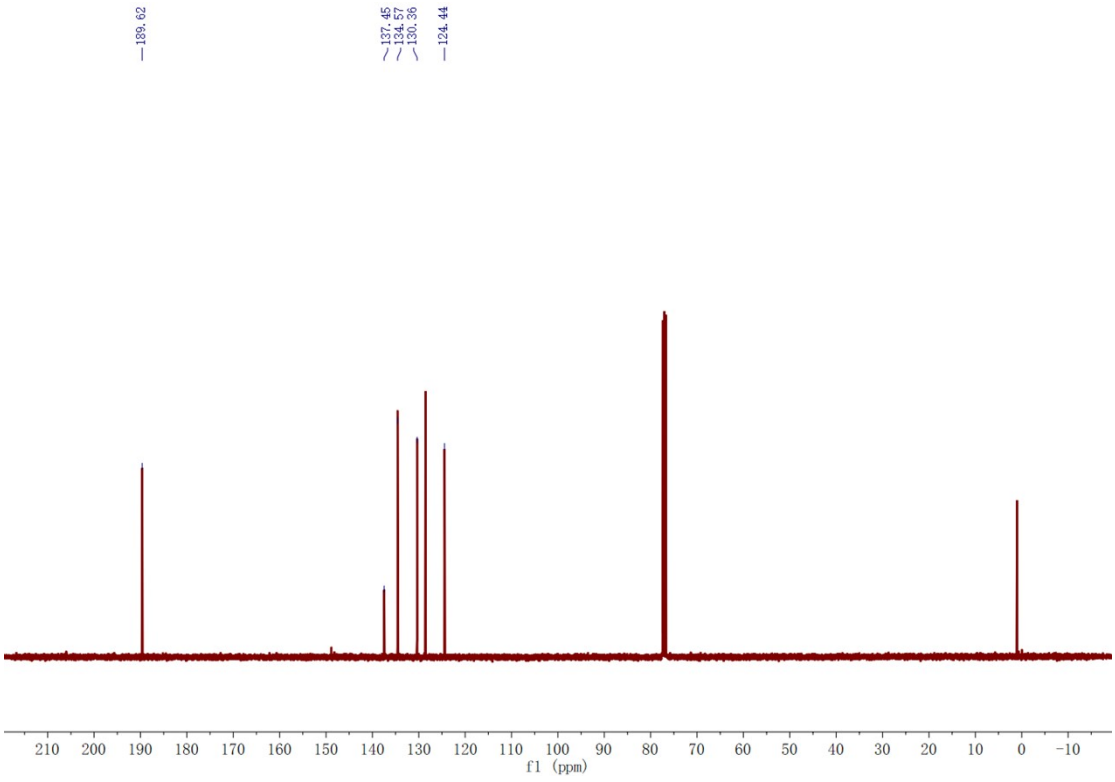

6. 2-naphthaldehyde： ^{1}H NMR (400 MHz, Chloroform-d) δ 10.19 (s, 1H), 8.36 (s, 1H), 8.05 – 7.91 (m, 4H), 7.64 (dt, J = 23.0, 7.0 Hz, 2H).^{13}C NMR (101 MHz, CDCl3) δ 192.16, 136.48, 134.46, 134.18, 132.69, 129.54, 129.09, 128.09, 127.09, 122.82.

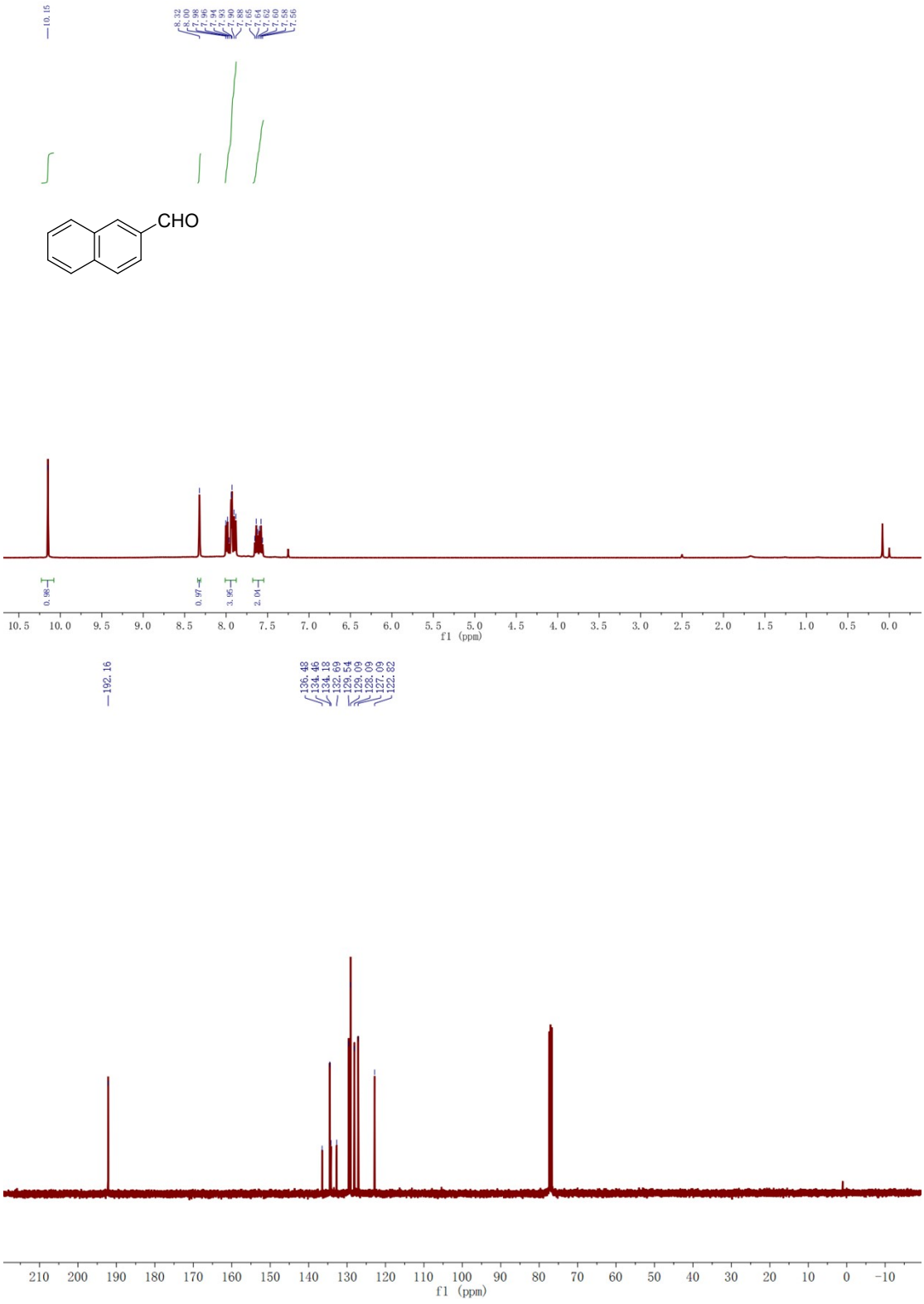

7. pyrene-4-carbaldehyde：^{1}H NMR (400 MHz, DMSO-d6) δ 10.23 (s, 1H), 8.65 (s, 1H), 8.23 (d, J = 8.1 Hz, 1H), 8.12 (dd, J = 14.3, 8.3 Hz, 2H), 7.97 (d, J = 8.4 Hz, 1H), 7.76 (dt, J = 23.4, 7.1 Hz, 2H). ^{13}C NMR (101 MHz, DMSO) δ 193.62, 167.76, 136.68, 135.00, 133.32, 133.27, 131.25, 129.92, 129.71, 129.59, 128.99.

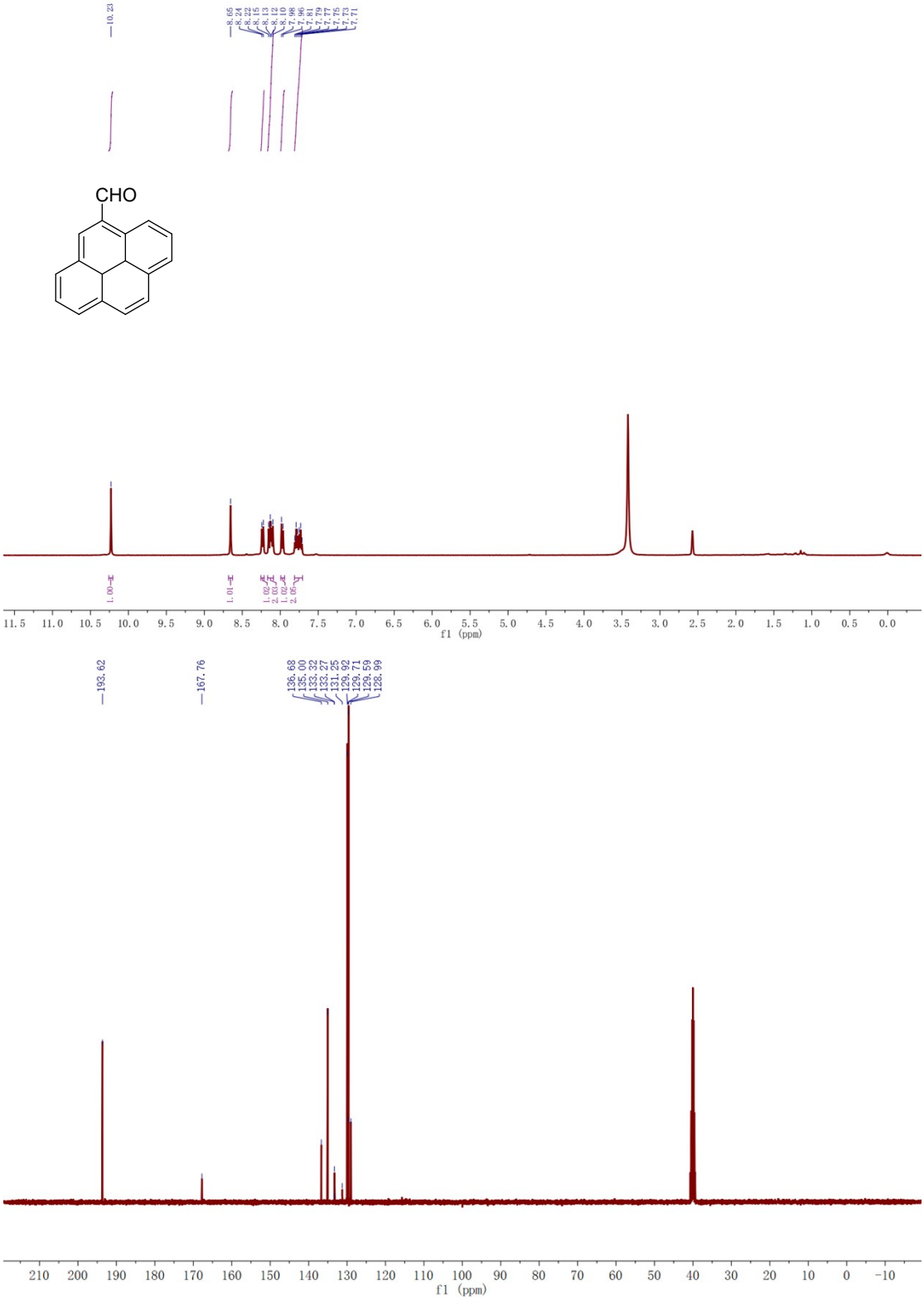

8. acetophenone：^{1}H NMR (400 MHz, Chloroform-d) δ 7.96 (d, J = 7.7 Hz, 2H), 7.56 (t, J = 7.4 Hz, 1H), 7.46 (t, J = 7.4 Hz, 2H), 2.60 (s, 3H). ^{13}C NMR (101 MHz, CDCl3) δ 198.13, 137.28, 133.18, 128.67, 128.40, 26.71.

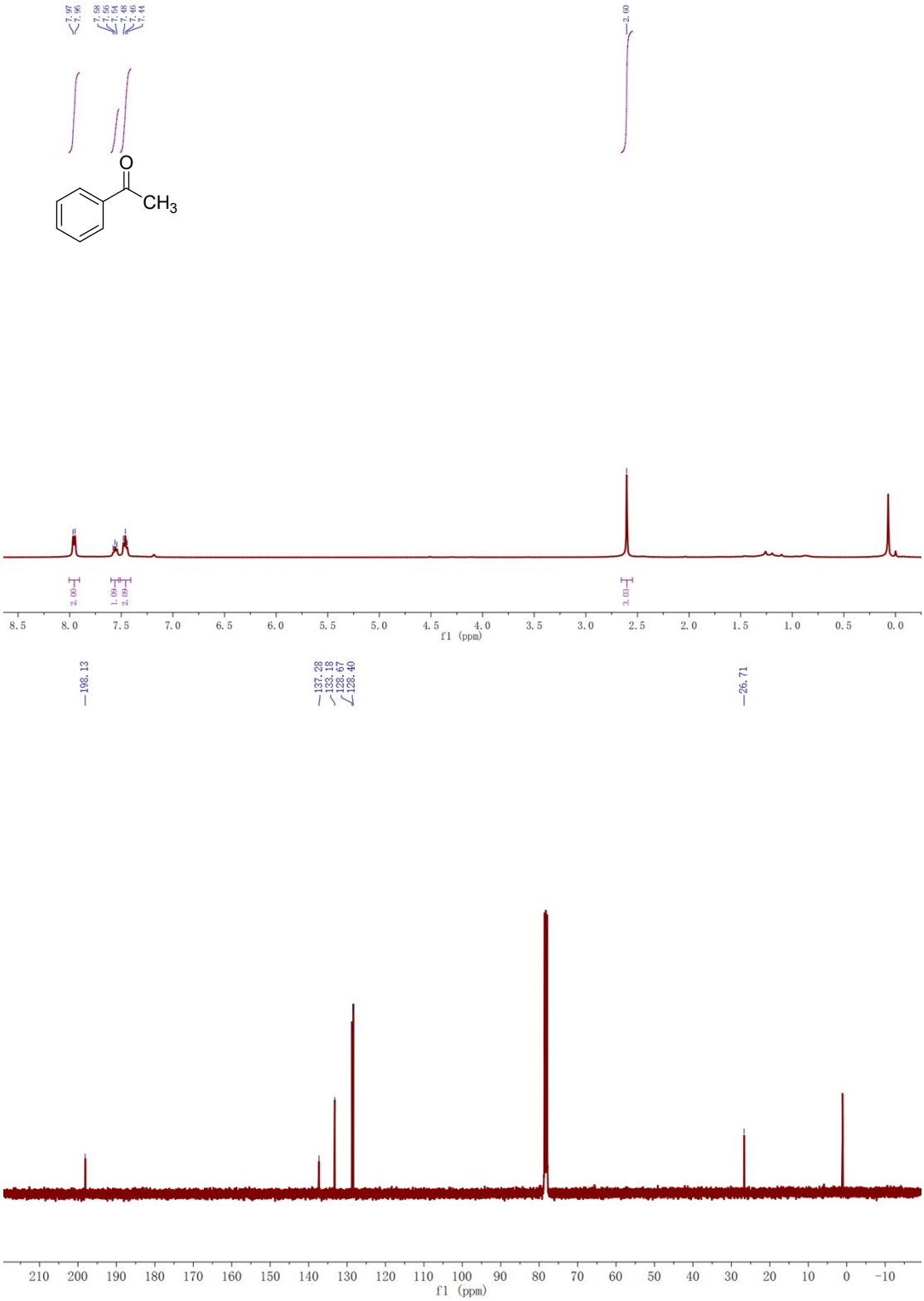

9. 1-(p-tolyl)ethan-1-one：^{1}H NMR (400 MHz,Chloroform-d) δ 7.85 (d, J = 7.7 Hz, 2H), 7.25 (d, J = 7.7 Hz, 2H), 2.57 (s, 3H), 2.41 (s, 3H). ^{13}C NMR (101 MHz, CDCl3) δ 197.79, 143.87, 134.84, 129.30, 128.50, 26.57, 21.69.

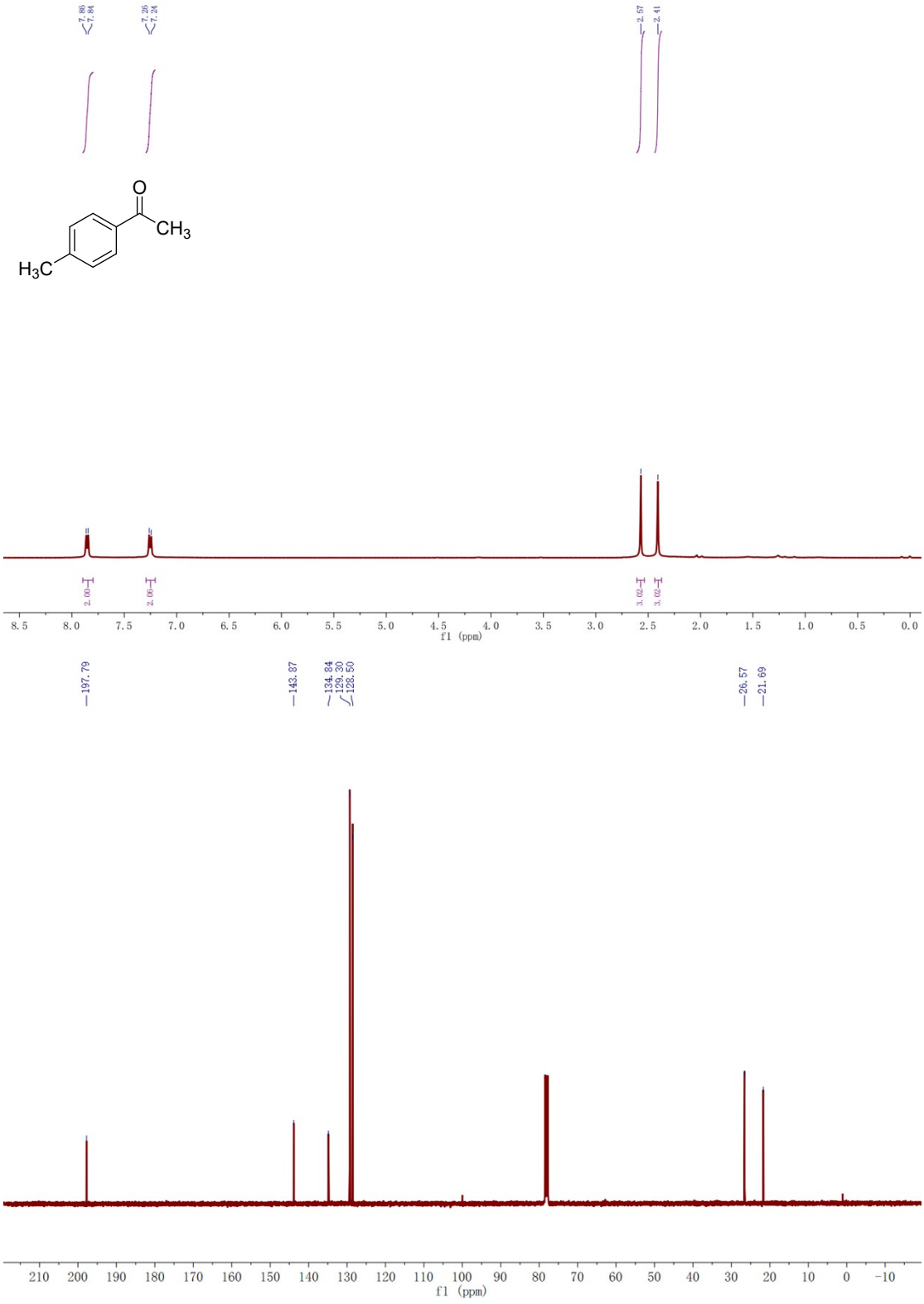

10. benzophenone：^{1}H NMR (400 MHz, Chloroform-d) δ 7.87 – 7.76 (m, 2H), 7.63 – 7.55 (m, 1H), 7.49 (q, J = 7.5 Hz, 2H). ^{13}C NMR (101 MHz, CDCl3) δ 196.68, 137.66, 132.37, 130.03, 128.26.